

The Energy Spectra of Electron Microbursts Between 200 keV and 1 MeV

A. T. Johnson¹, M. Shumko², J. Sample¹, B. Griffith³, D. Klumpar¹, H.
Spence⁴, J. B. Blake⁵

¹Physics Department, Montana State University, Bozeman, MT 59717, USA

²NASA's Goddard Space Flight Center, Greenbelt, MD 20771, USA

³Department of Earth and Space Sciences, University of Washington, Seattle, WA 98195, USA

⁴Physics Department, University of New Hampshire, Durham, NH 03824, USA

⁵Space Science Applications Laboratory, The Aerospace Corporation, El Segundo, CA 90245, USA

Key Points:

- We present a statistical study of the energy spectrum of electron microbursts observed by the FIREBIRD-II CubeSats.
- Individual microbursts contain more electrons at a higher AE, as well as relatively more high energy electrons.
- The microburst scattering mechanism is more efficient at scattering low energy electrons.

Corresponding author: Arlo Johnson, arlotjohnson@gmail.com

Abstract

This study investigates the energy spectrum of electron microbursts observed by the Focused Investigation of Relativistic Electron Burst: Intensity, Range, and Dynamics II (FIREBIRD-II) CubeSats. FIREBIRD-II is a pair of CubeSats, launched in January 2015 into a low Earth orbit, that focus on studying electron microbursts. High resolution electron data from FIREBIRD-II consists of 5 differential energy channels between 200 keV and 1 MeV and a >1 MeV integral channel. This covers an energy range that has not been well studied from low Earth orbit with good energy and time resolution. This study aims to improve understanding of the scattering mechanism behind electron microbursts by investigating their spectral properties and their relationship to the equatorial electron population under different geomagnetic conditions. Microbursts are identified in the region of the North Atlantic where FIREBIRD only observes electrons in the bounce loss cone. The electron flux and exponential energy spectrum of each microburst is calculated using a FIREBIRD instrument response modeled in GEANT4 (GEometry ANd Tracking) and compared with the near equatorial electron spectra measured by the Van Allen Probes. Microbursts occurring when the AE index is enhanced tend to carry more electrons with relatively higher energies. The microburst scattering mechanism is more efficient at scattering electrons with lower energies, however the difference in scattering efficiency between low and high energy is reduced during periods of enhanced AE.

1 Introduction

Microbursts are short intensifications of electron precipitation into the atmosphere lasting up to a few hundred milliseconds. The term microburst was first used by Anderson and Milton (1964) to describe enhancements in balloon observations of ≤ 100 keV bremsstrahlung X-Rays caused by electrons impacting the atmosphere. Later balloon observations up to 300 keV revealed microbursts to be a significant loss process in the dayside magnetosphere (Parks, 1978). More recently, relativistic (> 1 MeV) electron microbursts have been observed in situ by spacecraft (Imhof et al., 1992; J. Blake et al., 1996; Lorentzen, Blake, et al., 2001).

Microbursts are most likely generated through resonant interactions with whistler-mode chorus (Nakamura et al., 2000; Breneman et al., 2017). Previous studies have shown that microburst activity coincides with the time and location of whistler-mode chorus (Oliven & Gurnett, 1968; Lorentzen, Looper, & Blake, 2001; Lorentzen, Blake, et al., 2001; Lam et al., 2010) and that microbursts have a similar scale size to chorus wave regions (Shumko et al., 2020). In addition, theoretical studies have established the possible effectiveness of scattering by whistle-mode chorus (Chang & Inan, 1983; Rosenberg et al., 1990; Chen et al., 2020).

The importance of microbursts to the overall magnetospheric system could be significant. Using storm time Solar, Anomalous, and Magnetospheric Particle EXplorer (SAMPEX) Heavy Ion Large Telescope (HILT) data, it has been estimated that microbursts are capable of emptying the outer radiation belt of 1 MeV electrons on the order of a day (Lorentzen, Looper, & Blake, 2001; O'Brien et al., 2004; Thorne et al., 2005). This represents a significant source of electron loss from the magnetosphere.

An important factor to understand microbursts and their relationship to the magnetospheric system is the energy spectrum. Comparing the energy spectrum of a microburst to the background energy spectrum in the radiation belts gives insight into the processes that scatter microburst electrons and helps determine the importance of microbursts as a loss process at various energies. Previous studies of the microburst energy spectrum have focused on lower energy microbursts of 10's to a couple hundred keV (e.g. Anderson et al., 1966; Lampton, 1967; Reinard et al., 1997; Lee et al., 2005, 2012) or relativistic energies of > 1 MeV (e.g. Imhof et al., 1992) but the energy range from a few hundred keV to 1 MeV has not been well studied. J. Blake et al. (1996) compared microburst

68 detections on the 150 keV and > 1 MeV channels of the HILT detector on SAMPEX
 69 and found they were not always correlated, which could indicate a difference in gener-
 70 ation mechanism. Lorentzen, Blake, et al. (2001) showed that chorus propagating obliquely
 71 could explain why microbursts of different energies are not correlated despite having the
 72 same driver. To determine if the generation mechanism for microbursts with 10s of keV
 73 and MeV energies is different it's important to study the intervening energies.

74 This study uses microburst data from low Earth orbit collected by the Focused In-
 75 vestigation of Relativistic Electron Burst: Intensity, Range, and Dynamics II (FIREBIRD-
 76 II, hereafter FIREBIRD) CubeSat mission (Spence et al., 2012; Johnson et al., 2020) to
 77 investigate the energy spectrum of microbursts from 200 keV to 1 MeV. These spectra
 78 are compared with near equatorial observations by the Magnetic Electron Ion Spectrom-
 79 eter (MagEIS) aboard the Van Allen Probes (J. B. Blake et al., 2013) to estimate the
 80 efficiency of the scattering mechanism at different energies and levels of geomagnetic ac-
 81 tivity.

82 2 Instrument Description

83 FIREBIRD-II (Johnson et al., 2020) is a pair of National Science Foundation Cube-
 84 Sats termed Flight Unit (FU) 3 and FU4. They were launched on January 31, 2015 into
 85 a 98 degree inclination, 400km X 600km orbit. Each unit contains two silicon solid-state
 86 detectors referred to as the collimated and surface detectors. These detectors are iden-
 87 tical except for an aluminum collimator over the collimated detector which reduces the
 88 field of view and geometric factor of that detector. The surface detector on FU4 never
 89 functioned in orbit and the surface detector on FU3 began behaving anomalously around
 90 July 2015 so only the collimated data is used in this study. In the first few days of the
 91 mission the spacecraft were very near each other in space and were able to simultane-
 92 ously detect microbursts (Crew et al., 2016; Shumko et al., 2018). The spacecraft sep-
 93 arated beyond the scale size of a microburst within just a few days so for the purposes
 94 of this study the spacecraft were treated independently.

95 FIREBIRD produces far more data than can be practically downloaded so a cam-
 96 paign strategy is used. In each campaign the spacecraft takes data until memory is filled,
 97 typically about 3-4 weeks, then the instrument is turned off until a selected subset of data
 98 has been downloaded. Over the course of the mission FIREBIRD has been taking data
 99 around a third of the time with the remaining two thirds mostly used for downloading
 100 data. FIREBIRD produces a 6 second cadence data product for 2 of the energy chan-
 101 nels which is used in combination with geomagnetic activity and satellite conjunctions
 102 to select times of high resolution data to download. This results in a selection bias for
 103 the events chosen to be downloaded. It's difficult to be certain how this bias manifests
 104 but it's likely that weak or isolated microbursts will be underrepresented since they have
 105 a minimal effect on the 6 second data. Campaigns have been configured with time ca-
 106 dences of 12.5, 18.75, and 50 ms, with 18.75 ms most common in the early mission and
 107 50 ms most common in the later mission. In addition, starting with campaign 21 the en-
 108 ergy channel boundaries were shifted to cover the low energy range in finer resolution.
 109 This study uses data from campaigns 1-22 so campaigns with each cadence rate and en-
 110 ergy boundary selection are used for spectral calculations.

111 MagEIS (J. B. Blake et al., 2013) is an instrument suite aboard each of NASA's
 112 Van Allen Probes measuring electrons and ions. The Van Allen Probes were launched
 113 in August 2012 on a near geostationary transfer orbit which samples the near equato-
 114 rial radiation belts from about 600 km up to about $6 R_E$. Each probe spins with a pe-
 115 riod of about 11 seconds to sample different pitch angles. The MagEIS suite is composed
 116 of 4 instruments which collectively cover electron energies from about 20 keV to 4.8 MeV.
 117 This study uses the electron flux values from MagEIS in the range from 200 to 1200 keV
 118 to mimic the FIREBIRD energy range and in the pitch angle bin closest to the loss cone.

3 Event Selection

FIREBIRD high resolution data from campaigns 1-22 (February 2015 - May 2019) were analyzed for this study. Candidate events were identified using a wavelet transformation and filtering similar to the analysis described in Torrence and Compo (1998). The wavelet used in the transform is the Second Derivative of Gaussian which has a similar shape to a microburst. This wavelet is convolved with the data to create a power spectrum as a function of Fourier period and time. Microbursts with a similar width as the wavelet will convolve strongly and have a higher power. In order to detect a variety of possible microburst widths this analysis was performed several times with wavelet widths ranging from twice the data cadence up to 1 second.

An example of this process is shown in Figure 1. Figure 1a shows high resolution data from the 223.8 keV energy channel on FU4. Figure 1b shows the corresponding wavelet power spectrum. Times with possible microbursts are identified by filtering the wavelet spectrum to times of significant power lasting no longer than 1 second. The power is considered significant when it rises above the 95% confidence level of a red noise power spectrum, marked with bold contours in Figure 1b. The white hatched area in Figure 1b covers periods longer than 1 second. Times that meet both of these criteria are inverse transformed back to the time domain, shown in Figure 1c, and will be considered a microburst candidate if the time series is peaked and above a 0.1 count threshold. The peaks of identified microbursts are marked with stars in Figure 1a. This algorithm identified 11866 and 10789 microburst candidates on FU3 and FU4 respectively.

To reduce the effect of background precipitation and ensure observations were of recently scattered microbursts, these events were further restricted to the region of the North Atlantic conjugate to the South Atlantic Anomaly (SAA), often referred to as the Bounce Loss Cone (BLC) region, similar to previous studies (e.g. Dietrich et al., 2010; Comess et al., 2013). Particles observed at FIREBIRD's altitude in this region have a conjugate mirror point in the southern hemisphere below 100 km. Electrons in the BLC will interact with the atmosphere and eventually be lost, with electrons mirroring deeper in the atmosphere being lost in fewer bounces. Around 3/4 of the identified microbursts had a mirror altitude below 50 km and would have been lost within a couple bounce periods. The conjugate point of each candidate event was calculated using the Tsyganenko 1989 (T89) magnetic field model (Tsyganenko, 1989) keeping any event with a conjugate altitude below 100 km, a Latitude between 0 and 80, and Longitude between -90 and 60. These additional criteria are met by 1612 and 1256 candidate events on FU3 and FU4 respectively. The remaining candidate events were then independently reviewed by two authors and any events both agreed were microbursts were selected for this study. This leaves a final set of 400 microburst events on FU3 and 386 microburst events on FU4. Much of the following analysis utilizes the Auroral Electrojet (AE) index which was available through February 2018. There were 277 events on FU3 and 227 events on FU4 with AE data available.

4 Analysis

Each identified microburst was fit with an assumed exponential function. Figure 2 shows an example microburst observed by FU4 and the resulting fit. For each microburst the prominence was calculated, defined as the vertical distance between the peak and its lowest contour line. The lowest contour in the 251.5 keV channel appears as the horizontal red line on Figure 2a. This is considered the background level and is subtracted from the count data. To mitigate fluctuations due to Poisson noise, the counts are then integrated across the width of the peak at half prominence, which is equivalent to the full width at half maximum after the background subtraction. The dashed horizontal black line in Figure 2a represents the height of half prominence and the shaded area shows the integration boundaries.

170 The count rates were then converted to flux using the assumed exponential shape
 171 and the energy dependent geometric factors determined by the GEANT4 (GEometry ANd
 172 Tracking) (Agostinelli et al., 2003) FIREBIRD mass model described in Johnson et al.
 173 (2020). The flux was first estimated from the counts by dividing by an approximate ge-
 174 ometric factor and the energy bin width. An exponential flux function of the form $J(E) =$
 175 $J_0 e^{-(E/E_0)}$ was then fit to these fluxes, where $J(E)$ is the flux at energy E , J_0 is a mea-
 176 sure of intensity, and E_0 is the e-folding energy. The fitted function was then integrated
 177 with the GEANT determined geometric factors to model the counts that FIREBIRD would
 178 observe. The parameters of the flux function were then iterated to find the best agree-
 179 ment between the observed and modeled count rates.

180 Figure 2b shows the GEANT determined flux values in the 5 differential energy chan-
 181 nels and the best fit function. To calculate the flux in each energy channel, an effective
 182 geometric factor is first found by dividing the modeled count rates by the value of the
 183 flux function at the center of the energy channel. The observed count rates and their Pois-
 184 son error are then divided by this effective geometric factor and shown as the black points
 185 and error bars in Figure 2b. The distribution of E_0 and J_0 is shown in Figure 3 for all
 186 microbursts with AE data and will be described in the next section.

187 MagEIS data from 200 to 1200 keV were used to investigate the energy spectrum
 188 of the source equatorial electrons. For each microburst observed on FIREBIRD a cor-
 189 responding energy spectrum was found on each Van Allen Probe. Times of MagEIS data
 190 to analyze were selected as the nearest crossing of the microburst’s L shell at any MLT
 191 separation or time difference. Most events were associated with a time difference between
 192 observations of less than 2 hours, although a handful were up to 5 hours. The MLT sep-
 193 aration was found to be anywhere between -12 to +12 hours, but with a peak between
 194 +/- 1 hour due to the preference of the FIREBIRD team to download data during con-
 195 junctions with the Van Allen Probes. For this study the pitch-angle resolved flux data
 196 from the pitch angle bin nearest to 0 degrees (northward electrons) were used. When data
 197 near 0 degrees were unavailable the data from the pitch angle bin nearest to 180 degrees
 198 were used instead in order to sample the trapped population nearest to the loss cone,
 199 and therefore the population most likely to be scattered into a microburst. The anal-
 200 ysis was also performed with the spin-averaged MagEIS count data which yielded sim-
 201 ilar results.

202 The MagEIS flux data were then fit with an assumed exponential flux function for
 203 comparison to FIREBIRD. The most common spectral shapes observed by MagEIS are
 204 exponential, power law, and bump-on-tail with exponential spectra dominating in the
 205 outer radiation belt outside of the plasmopause (Zhao et al., 2019). The plasmopause
 206 location was calculated for each microburst event using the plasmopause model from O’Brien
 207 and Moldwin (2003) and the AE index. According to this model all of the microburst
 208 events occurred outside the plasmopause, and most occurred at least 1 L from the plasma-
 209 pause, so the assumption of an exponential spectral shape is not unreasonable. To fil-
 210 ter any non-exponential spectral shapes the standard deviation error is calculated for
 211 E_0 in each fit and must be less than 15% to be included.

212 5 Discussion

213 The distributions of the microbursts in the intensity J_0 and e-folding energy E_0
 214 are shown in Figure 3. Each microburst is colored according to the value of the AE in-
 215 dex at the time of the burst. Figures 3a and 3c are histograms for each parameter show-
 216 ing the relative occurrence rate for each AE value with the gray bars representing all mi-
 217 crobursts. Each AE bin in the histogram has been normalized by the number of events
 218 in the bin. The solid lines in Figure 3b are contours representing the total number of elec-
 219 trons across all energies that would be observed by FIREBIRD. The total counts are de-
 220 termined by applying the FIREBIRD GEANT model to the exponential flux function

221 for a given E_0 and J_0 pair and summing the response of all energy channels. Contours
 222 are drawn at 1, 20, 40, and 80 thousand counts per second.

223 The low J_0 boundary of the spectral distribution in Figure 3b appears to follow
 224 the 1000 count per second contour line. It's likely this boundary arises from the sensi-
 225 tivity floor of the FIREBIRD instruments. As a comparison, Lee et al. (2005) used data
 226 from STSAT-1 to characterize the energy spectrum of microbursts between 170-330 keV
 227 with 30 energy channels. Lee et al. (2005) measured an E_0 of 19-20 keV in quiet con-
 228 ditions and 39-41 keV in storm times. An E_0 of 40 keV is at the low end of the distri-
 229 bution observed on FIREBIRD, but no events with an E_0 below 30 keV were observed.
 230 For a microburst with a 20 keV e-folding energy to deposit enough counts to be observed
 231 on FIREBIRD, assumed here to be 1000 counts/second, a J_0 around 10^6 would be re-
 232 quired. It's possible the lowered FIREBIRD energy channel boundaries beginning in cam-
 233 paign 21 would be sensitive to microbursts with a lower E_0 but there were not enough
 234 events in campaigns 21 and 22 to get a statistically significant result.

235 The high J_0 boundary of the distribution in Figure 3b does not follow the count
 236 contour lines. At an E_0 of 50 keV the bursts with the highest J_0 are near the 20,000 count/second
 237 contour, but at an E_0 of 150 keV almost 80,000 counts per second can be observed in
 238 the most intense bursts. This increase in electrons contained in a microburst could be
 239 explained by an increase in source electrons near the equator to be scattered or an im-
 240 provement in the scattering efficiency of the microburst generation mechanism as AE in-
 241 creases, or some combination of the two. If this boundary were due to instrumental ef-
 242 fects the opposite trend would be expected. Events observed by FIREBIRD are processed
 243 via a Wilkinson rundown Analog-Digital Converter with a dead time proportional to the
 244 energy deposited into the detector by the event. Therefore, at times with relatively more
 245 high energy electrons the total number of electrons needed to reach the saturation limit
 246 on FIREBIRD is reduced.

247 The distribution in Figure 3 varies with the AE index. Microbursts that occur dur-
 248 ing times of high AE tend to have a higher E_0 than microbursts at a lower AE with a
 249 similar J_0 , and microbursts with a similar E_0 tend to have a higher J_0 at high AE. This
 250 is also reflected in Figure 3b by high AE microbursts carrying more electrons. The his-
 251 tograms in Figures 3a and 3c show this trend as well, although it's blurred due to look-
 252 ing at microbursts of all E_0 or J_0 instead of a specific value.

253 There is substantial overlap between the AE bins suggesting there may be other
 254 compounding effects that have not been accounted for. Variations based on L or MLT
 255 were investigated separately but no clear pattern was found. A possibility that cannot
 256 be investigated by FIREBIRD is a dependence on pitch angle. If the microburst scat-
 257 tering mechanism is able to scatter certain energies deeper into the loss cone the energy
 258 spectrum would develop a dependence on pitch angle. FIREBIRD experiences a slow tum-
 259 ble which causes it to sample a range of pitch angles. The precise nature of the tumble
 260 is unknown, and there is no pointing information to quantify it, so it's unclear what pitch
 261 angles are being sampled.

262 To further investigate the nature of the microburst scattering mechanism, the en-
 263 ergy spectrum observed on FIREBIRD was compared with MagEIS aboard the Van Allen
 264 Probes. Microburst electrons are rapidly scattered from the trapped population of elec-
 265 trons near the loss cone so comparing their spectra can reveal properties of the scatter-
 266 ing mechanism. Figure 4 shows a comparison of both E_0 and J_0 and highlights how the
 267 relationship changes with AE. Figures 4a and 4b compare E_0 and Figures 4c and 4d com-
 268 pare J_0 . Panels on the left (4a and 4c) highlight points observed at AE < 200 in red while
 269 panels on the right (4b and 4d) highlight points at AE > 500. The dashed line in each
 270 panel indicates where the parameters are equal.

271 Almost every observed microburst in Figures 4a and 4b appears above the dashed
 272 line indicating a lower E_0 was observed on FIREBIRD than on MagEIS. This suggests
 273 the microburst scattering mechanism is more efficient at scattering lower energy elec-
 274 trons. Furthermore, microbursts observed during times of higher AE in Figure 4b have
 275 a closer agreement in E_0 between the two missions. Considering a higher AE is also as-
 276 sociated with more total electrons (Figure 3) this likely indicates that the scattering mech-
 277 anism becomes more efficient at scattering high energy electrons as AE increases.

278 Figures 4c and 4d show all points above the dashed line indicating more electron
 279 flux near the equator than in the microbursts. Comparing Figure 4c with 4d shows that
 280 a higher AE is associated with an enhanced J_0 on both instruments, although the en-
 281 hancement is more pronounced on MagEIS. This indicates a larger trapped electron pop-
 282 ulation which could explain the increased number of counts associated with higher AE
 283 in Figure 3.

284 6 Conclusion

285 We have presented a statistical study of the energy spectrum of microburst elec-
 286 trons between 200 keV and 1 MeV. Microbursts were identified on the FIREBIRD-II Cube-
 287 Sats and fit with an exponential energy spectrum. Using MagEIS data the microburst
 288 spectrum was compared with the spectrum of the source population near the equator.
 289 The microburst fit parameters and their relationship to the equatorial population was
 290 tested against MLT, L shell, and AE index.

291 We found no correlation between either E_0 or J_0 and MLT, or L shell, but an in-
 292 crease in AE index is associated with an increase in both parameters. This increase is
 293 also reflected as an increase in the number of electrons in an individual microburst. A
 294 comparison of the microburst and source e-folding energies found microbursts typically
 295 have a smaller E_0 , but an enhanced AE brought the e-folding energies into closer agree-
 296 ment. The values of J_0 for microbursts and the source population were also compared
 297 and it was found that an enhanced AE cause an increase in both the microburst J_0 and
 298 the source population J_0 .

299 Acknowledgments

300 FIREBIRD-II is supported by the National Science Foundation under Grant Nos. 0838034,
 301 1339414, and 1035642. FIREBIRD-II data are publicly available at
 302 http://solar.physics.montana.edu/FIREBIRD_II/. Processing and analysis of the MagEIS
 303 data was supported by Energetic Particle, Composition, and Thermal Plasma (RBSP-
 304 ECT) investigation funded under NASAs Prime contract no. NAS5-01072. All RBSP-
 305 ECT data are publicly available at the Web site <http://www.RBSP-ect.lanl.gov/>. The
 306 AE index used in this paper was provided by the WDC for Geomagnetism, Kyoto
 307 (<http://wdc.kugi.kyoto-u.ac.jp/wdc/Sec3.html>). A.T. Johnson was supported under NASA
 308 grant Nos. 80NSSC19K0265 and 80NSSC19K0842. M. Shumko acknowledges the sup-
 309 port provided by the NASA Postdoctoral Program at the NASAs Goddard Space Flight
 310 Center, administered by Universities Space Research Association under contract with
 311 NASA. The wavelet code for identifying microbursts was adapted from code written by
 312 Evgeniya Predybaylo, available at https://github.com/chris-torrence/wavelets/tree/master/wave_python.

313 References

314 Agostinelli, S., Allison, J., Amako, K., Apostolakis, J., Araujo, H., Arce, P., . . .
 315 Zschesche, D. (2003). GEANT4 - A simulation toolkit. *Nuclear Instru-*
 316 *ments and Methods in Physics Research, Section A: Accelerators, Spec-*
 317 *trometers, Detectors and Associated Equipment*, 506(3), 250–303. doi:
 318 10.1016/S0168-9002(03)01368-8

- 319 Anderson, K. A., Chase, L. M., Hudson, H. S., Lampton, M., Milton, D. W., &
 320 Parks, G. K. (1966). Balloon and rocket observations of auroral-zone
 321 microbursts. *Journal of Geophysical Research*, *71*(19), 4617–4629. doi:
 322 10.1029/jz071i019p04617
- 323 Anderson, K. A., & Milton, D. W. (1964). Balloon Observations of X Rays in the
 324 Auroral Zone 3. *Journal of Geophysical Research*, *69*(21).
- 325 Blake, J., Looper, M., Baker, D., Nakamura, R., Klecker, B., & Hovestadt, D. (1996,
 326 jan). New high temporal and spatial resolution measurements by SAMPEX of
 327 the precipitation of relativistic electrons. *Advances in Space Research*, *18*(8),
 328 171–186. Retrieved from [http://linkinghub.elsevier.com/retrieve/pii/](http://linkinghub.elsevier.com/retrieve/pii/0273117795009698)
 329 [0273117795009698](http://www.sciencedirect.com/science/article/pii/0273117795009698) [http://www.sciencedirect.com/science/article/pii/](http://www.sciencedirect.com/science/article/pii/0273117795009698)
 330 [0273117795009698](http://www.sciencedirect.com/science/article/pii/0273117795009698) doi: 10.1016/0273-1177(95)00969-8
- 331 Blake, J. B., Carranza, P. A., Claudepierre, S. G., Clemmons, J. H., Crain, W. R.,
 332 Dotan, Y., ... Zakrzewski, M. P. (2013). The Magnetic Electron Ion Spec-
 333 trometer (MagEIS) instruments aboard the Radiation Belt Storm Probes
 334 (RBSP) spacecraft. *The Van Allen Probes mission*, *9781489974*, 383–421. doi:
 335 10.1007/978-1-4899-7433-4-12
- 336 Breneman, A. W., Crew, A., Sample, J., Klumpar, D., Johnson, A., Agapitov,
 337 O., ... Kletzing, C. A. (2017). Observations Directly Linking Relativis-
 338 tic Electron Microbursts to Whistler Mode Chorus: Van Allen Probes and
 339 FIREBIRD II. *Geophysical Research Letters*, *44*(22), 11,265–11,272. doi:
 340 10.1002/2017GL075001
- 341 Chang, H. C., & Inan, U. S. (1983). Quasi-Relativistic Electron Precipitation Due
 342 to Interactions With Coherent VLF Waves in the Magnetosphere. *Journal of*
 343 *Geophysical Research*, *88*(A1), 318–328.
- 344 Chen, L., Breneman, A. W., Xia, Z., & Zhang, X.-j. (2020). Modeling of bounc-
 345 ing electron microbursts induced by ducted chorus waves. , 1–26. doi: 10.1029/
 346 2020GL089400
- 347 Comess, M. D., Smith, D. M., Selesnick, R. S., Millan, R. M., & Sample, J. G.
 348 (2013). Duskside relativistic electron precipitation as measured by SAMPEX:
 349 A statistical survey. *Journal of Geophysical Research: Space Physics*, *118*(8),
 350 5050–5058. doi: 10.1002/jgra.50481
- 351 Crew, A. B., Spence, H. E., Blake, J. B., Klumpar, D. M., Larsen, B. A., O'Brien,
 352 T. P., ... Widholm, M. (2016). First multipoint in situ observations of
 353 electron microbursts: Initial results from the NSF FIREBIRD II mission.
 354 *Journal of Geophysical Research: Space Physics*, *121*(6), 5272–5283. doi:
 355 10.1002/2016JA022485
- 356 Dietrich, S., Rodger, C. J., Clilverd, M. A., Bortnik, J., & Raita, T. (2010, dec).
 357 Relativistic microburst storm characteristics: Combined satellite and ground-
 358 based observations. *Journal of Geophysical Research*, *115*(A12), n/a–n/a.
 359 Retrieved from <http://doi.wiley.com/10.1029/2010JA015777> doi:
 360 10.1109/URSIGASS.2011.6051070
- 361 Imhof, W. L., Voss, H. D., Mobilia, J., Datlowe, D. W., Gaines, E. E., McGlen-
 362 non, J. P., & Inan, U. S. (1992). Relativistic electron microbursts. *Jour-
 363 nal of Geophysical Research*, *97*(A9), 13829. Retrieved from [http://](http://adsabs.harvard.edu/abs/1992JGR...9713829I)
 364 adsabs.harvard.edu/abs/1992JGR...9713829I doi: 10.1029/92JA01138
- 365 Johnson, A. T., Shumko, M., Griffith, B., Klumpar, D. M., Sample, J., Springer, L.,
 366 ... Blake, J. B. (2020). The FIREBIRD-II CubeSat mission: Focused inves-
 367 tigation of relativistic electron burst intensity, range, and dynamics. *Review*
 368 *of Scientific Instruments*, *91*(3). Retrieved from [https://doi.org/10.1063/](https://doi.org/10.1063/1.5137905)
 369 [1.5137905](https://doi.org/10.1063/1.5137905) doi: 10.1063/1.5137905
- 370 Lam, M. M., Horne, R. B., Meredith, N. P., Glauert, S. A., Moffat-Griffin, T., &
 371 Green, J. C. (2010). Origin of energetic electron precipitation ≥ 30 keV into
 372 the atmosphere. *Journal of Geophysical Research A: Space Physics*, *115*(A4),
 373 1–15. doi: 10.1029/2009JA014619

- 374 Lampton, M. (1967). Daytime Observations of Energetic Auroral-Zone Electrons.
375 *Journal of Geophysical Research*, *72*(23), 5817–5823.
- 376 Lee, J. J., Parks, G. K., Lee, E., Tsurutani, B. T., Hwang, J., Cho, K. S., ... Mc-
377 Carthy, M. P. (2012). Anisotropic pitch angle distribution of 100 keV mi-
378 croburst electrons in the loss cone: Measurements from STSAT-1. *Annales*
379 *Geophysicae*, *30*(11), 1567–1573. doi: 10.5194/angeo-30-1567-2012
- 380 Lee, J. J., Parks, G. K., Min, K. W., Kim, H. J., Park, J., Hwang, J., ... Park,
381 H. Y. (2005). Energy spectra of ~170-360 keV electron microbursts measured
382 by the Korean STSAT-1. *Geophysical Research Letters*, *32*(13), 1–4. doi:
383 10.1029/2005GL022996
- 384 Lorentzen, K. R., Blake, J. B., Inan, U. S., & Bortnik, J. (2001, apr). Obser-
385 vations of relativistic electron microbursts in association with VLF cho-
386 rus. *Journal of Geophysical Research*, *106*(A), 6017–6028. Retrieved from
387 <http://doi.wiley.com/10.1029/2000JA003018>[http://adsabs.harvard](http://adsabs.harvard.edu/cgi-bin/nph-data_query?bibcode=2001JGR...106.6017L&link_type=ABSTRACT%5Cnpapers3://publication/doi/10.1029/2000JA003018)
388 [.edu/cgi-bin/nph-data_query?bibcode=2001JGR...106.6017L&link_type=](http://adsabs.harvard.edu/cgi-bin/nph-data_query?bibcode=2001JGR...106.6017L&link_type=ABSTRACT%5Cnpapers3://publication/doi/10.1029/2000JA003018)
389 [ABSTRACT%5Cnpapers3://publication/doi/10.1029/2000JA003018](http://adsabs.harvard.edu/cgi-bin/nph-data_query?bibcode=2001JGR...106.6017L&link_type=ABSTRACT%5Cnpapers3://publication/doi/10.1029/2000JA003018) doi:
390 10.1029/2000JA003018
- 391 Lorentzen, K. R., Looper, M. D., & Blake, J. B. (2001, jul). Relativistic electron
392 microbursts during the GEM storms. *Geophysical Research Letters*, *28*(13),
393 2573–2576. Retrieved from <http://doi.wiley.com/10.1029/2001GL012926>
394 doi: 10.1029/2001GL012926
- 395 Nakamura, R., Isowa, M., Kamide, Y., Baker, D. N., Blake, J. B., & Looper, M.
396 (2000). SAMPEX observations of precipitation bursts in the outer radiation
397 belt. *Journal of Geophysical Research: Space Physics*, *105*(A7), 15875–15885.
398 doi: 10.1029/2000ja900018
- 399 O'Brien, T. P., Looper, M. D., & Blake, J. B. (2004). Quantification of relativis-
400 tic electron microburst losses during the GEM storms. *Geophysical Research*
401 *Letters*, *31*(4), L04802. Retrieved from [http://doi.wiley.com/10.1029/](http://doi.wiley.com/10.1029/2003GL018621)
402 [2003GL018621](http://doi.wiley.com/10.1029/2003GL018621) doi: 10.1029/2003GL018621
- 403 O'Brien, T. P., & Moldwin, M. B. (2003). Empirical plasmopause mod-
404 els from magnetic indices. *Geophysical Research Letters*, *30*(4). doi:
405 10.1029/2002GL016007
- 406 Oliven, M. N., & Gurnett, D. A. (1968). Microburst phenomena: 3. An association
407 between microbursts and VLF chorus. *Journal of Geophysical Research*, *73*(7),
408 2355–2362. doi: 10.1029/ja073i007p02355
- 409 Parks, G. K. (1978). Microburst Precipitation Phenomena. *Journal of Geomag-*
410 *netism and Geoelectricity*, *30*.
- 411 Reinard, A. A., Skoug, R. M., Datta, S., & Parks, G. K. (1997). Energy spec-
412 tral characteristics of auroral electron microburst precipitation. *Geophysical*
413 *Research Letters*, *24*(5), 611–614. doi: 10.1029/97GL00377
- 414 Rosenberg, T. J., Wei, R., Detrick, D. L., & Inan, U. S. (1990). Observations and
415 Modeling of Wave-Induced Microburst Electron Precipitation. *Journal of Geo-*
416 *physical Research*, *95*, 6467–6475.
- 417 Shumko, M., Johnson, A. T., Sample, J. G., Griffith, B. A., Turner, D. L., O'Brien,
418 T. P., ... Claudepierre, S. G. (2020). Electron Microburst Size Distribution
419 Derived With AeroCube-6. *Journal of Geophysical Research: Space Physics*,
420 *125*(3). doi: 10.1029/2019JA027651
- 421 Shumko, M., Sample, J., Johnson, A., Blake, J. B., Crew, A., Spence, H., ... Han-
422 dley, M. (2018). Microburst Scale Size Derived from Multiple Bounces of a
423 Microburst Simultaneously Observed with the FIREBIRD-II CubeSats. *Geo-*
424 *physical Research Letters*.
- 425 Spence, H. E., Blake, J. B., Crew, A. B., Driscoll, S., Klumpar, D. M., Larsen,
426 B. A., ... Widholm, M. (2012). Focusing on size and energy dependence
427 of electron microbursts from the Van Allen radiation belts. *Space Weather*,
428 *10*(11), 10–12. doi: 10.1029/2012SW000869

- 429 Thorne, R. M., O'Brien, T. P., Shprits, Y. Y., Summers, D., & Horne, R. B.
430 (2005, sep). Timescale for MeV electron microburst loss during geomag-
431 netic storms. *Journal of Geophysical Research: Space Physics*, *110*(A9).
432 Retrieved from <http://doi.wiley.com/10.1029/2004JA010882> doi:
433 10.1029/2004JA010882
- 434 Torrence, C., & Compo, G. P. (1998). A Practical Guide to Wavelet Analysis. *Bul-*
435 *letin of the American Meteorological Society*, *79*(1), 61–78. doi: 10.1175/1520-
436 -0477(1998)079(0061:APGTWA)2.0.CO;2
- 437 Tsyganenko, N. A. (1989). A magnetospheric magnetic field model with a warped
438 tail current sheet. *Planetary and Space Science*, *37*(1), 5–20. doi: 10.1016/
439 0032-0633(89)90066-4
- 440 Zhao, H., Johnston, W. R., Baker, D. N., Li, X., Ni, B., Jaynes, A. N., . . . Boyd,
441 A. J. (2019). Characterization and Evolution of Radiation Belt Elec-
442 tron Energy Spectra Based on the Van Allen Probes Measurements. *Jour-*
443 *nal of Geophysical Research: Space Physics*, *124*(6), 4217–4232. doi:
444 10.1029/2019JA026697

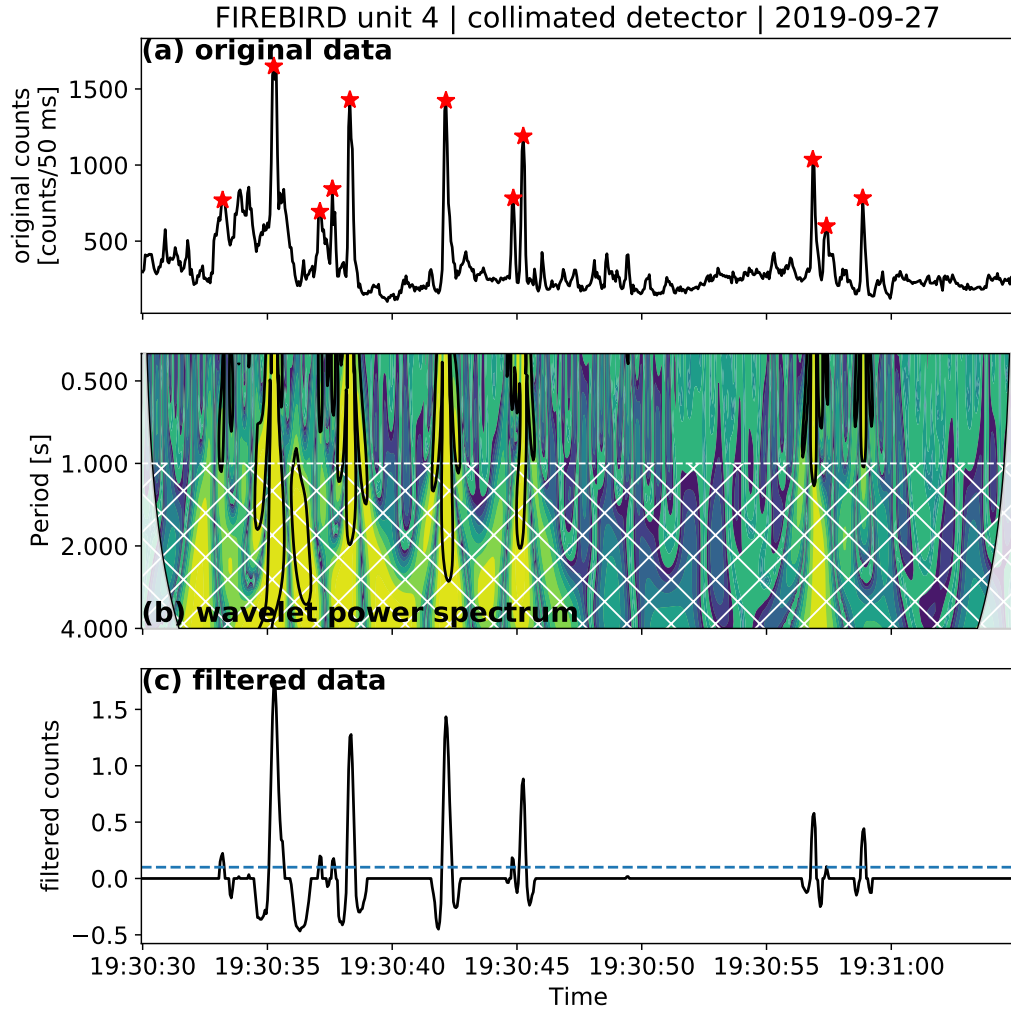


Figure 1. An example of the wavelet detection algorithm used to identify microbursts. a) Original data from the 223.8 keV energy channel of FU4. Stars mark the peaks of identified microbursts. b) The wavelet power spectrum of the data. Regions where the wavelet power spectrum exceeds the 95% confidence level of a red noise power spectrum are shown with bold contours. The white hatched region has Fourier periods longer than 1 second and are filtered out. c) The filtered wavelet spectrum transformed back to the time domain. Times that exceed a threshold of 0.1, shown by the horizontal dashed line, are considered microbursts.

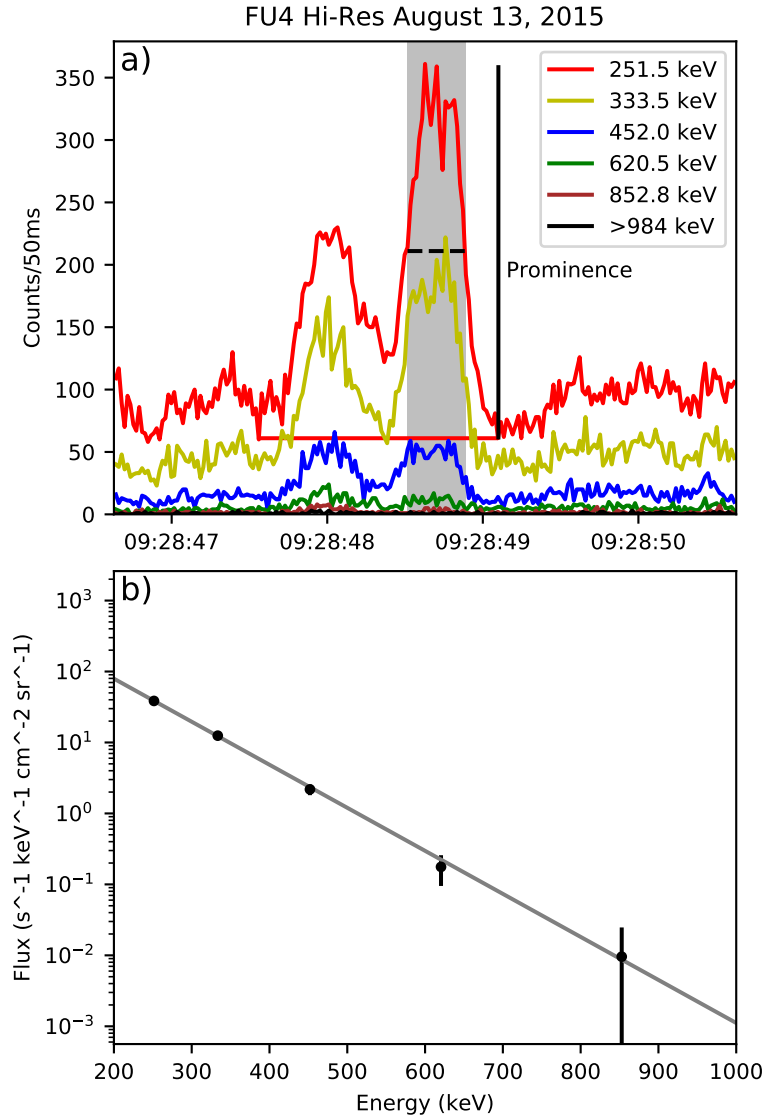


Figure 2. Example microburst and fit energy spectrum. Panel a) shows the FIREBIRD time series data. The shaded gray area represents the time range the microburst was integrated over, calculated at half prominence as shown with the dashed horizontal black line. The horizontal red line represents the background levels for the 251.5 keV channel. Panel b) shows the GEANT determined flux in each energy channel and best fit e-folding function.

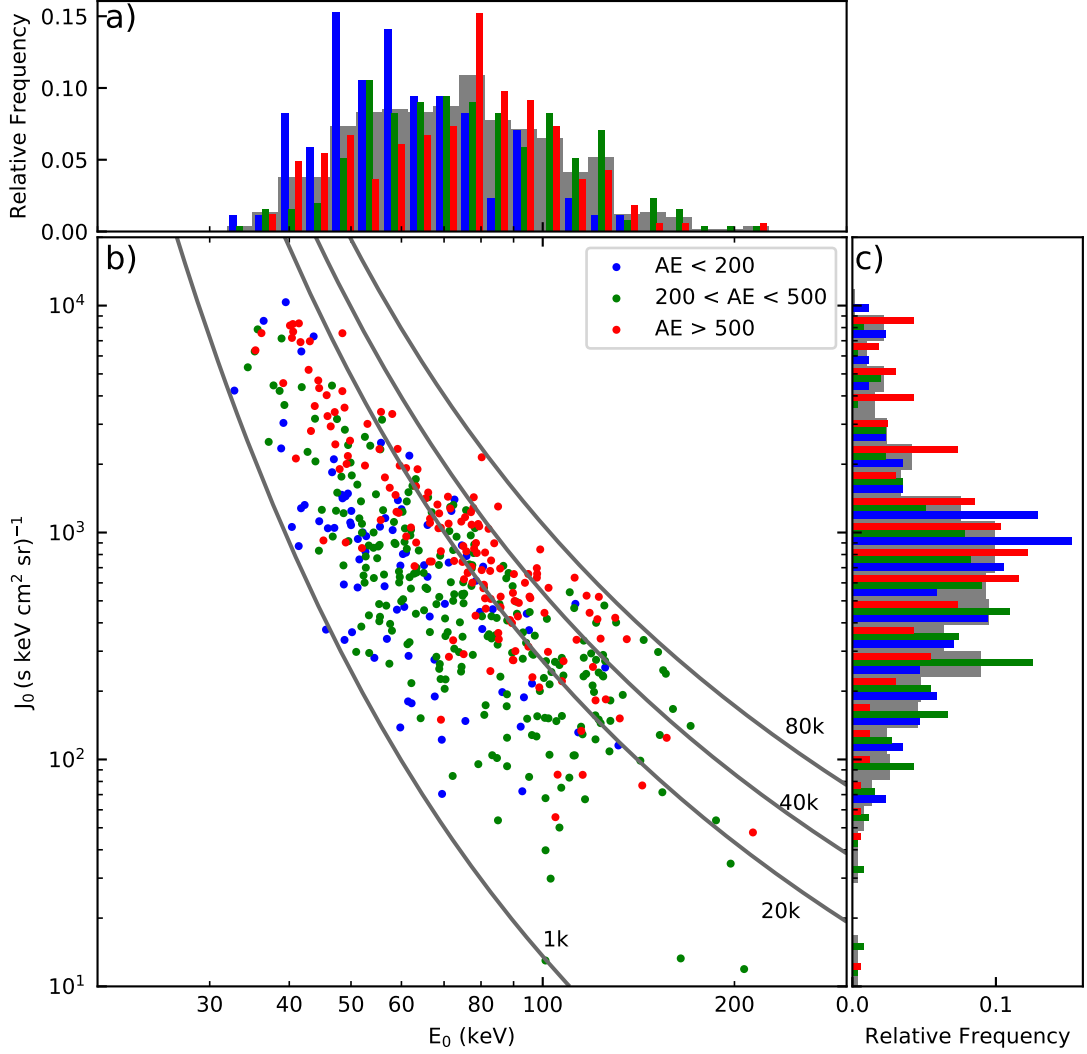


Figure 3. Comparison of E_0 and J_0 for each microburst with AE data in the study. Panel a) shows a histogram of E_0 and panel c) shows a histogram of J_0 . The histograms are normalized by the number of microbursts in each AE bin. The gray bars in back show the distribution for all microbursts. Panel b) shows the value of E_0 and J_0 for each microburst. The solid lines in panel b) show contours of constant total counts per second. Contours are at 1, 20, 40, and 80 thousand counts per second.

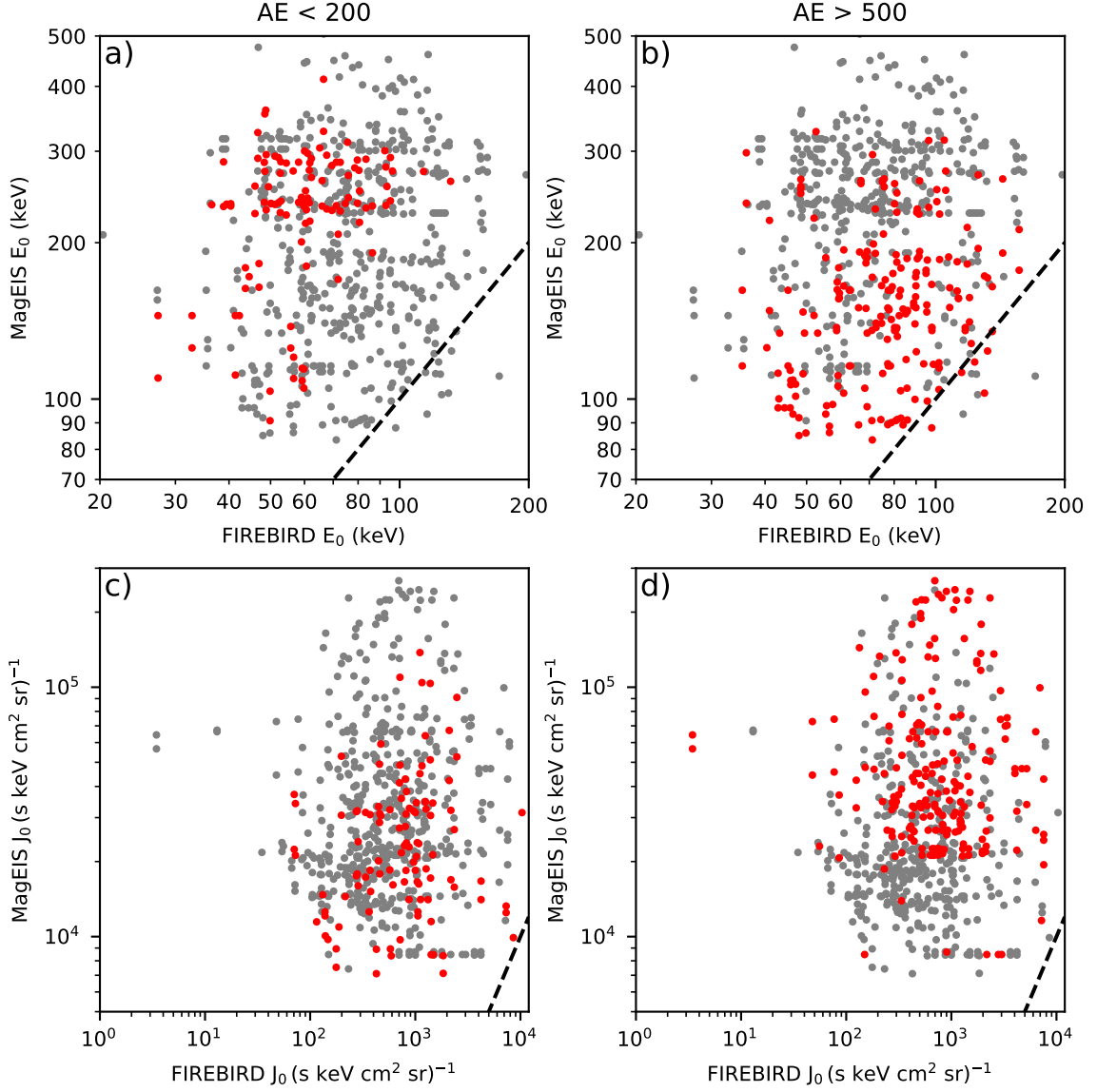


Figure 4. Comparison of E_0 and J_0 between FIREBIRD and MagEIS. Panels a) and b) show a comparison of E_0 and panels c) and d) show a comparison of J_0 . Each panel has points highlighted in red according to an AE filter, with panels a) and c) showing $\text{AE} < 200$ and panels b) and d) showing $\text{AE} > 500$. The dashed line in each panel indicates where the parameters are equal.